

3D Compression Using Neural Fields

Janis Postels¹ Yannick Strümppler² Klara Reichard³ Luc Van Gool¹ Federico Tombari^{2,3}
¹ETH Zurich ²Google ³Technical University Munich
{jpostels, vangool}@vision.ee.ethz.ch klara.reichard@tum.de
{strumpler, tombari}@google.com

Abstract

Neural Fields (NFs) have gained momentum as a tool for compressing various data modalities - e.g. images and videos. This work leverages previous advances and proposes a novel NF-based compression algorithm for 3D data. We derive two versions of our approach - one tailored to watertight shapes based on Signed Distance Fields (SDFs) and, more generally, one for arbitrary non-watertight shapes using Unsigned Distance Fields (UDFs). We demonstrate that our method excels at geometry compression on 3D point clouds as well as meshes. Moreover, we show that, due to the NF formulation, it is straightforward to extend our compression algorithm to compress both geometry and attribute (e.g. color) of 3D data.

1. Introduction

It becomes increasingly important to transmit 3D content over band-limited channels. Consequently, there is a growing interest in algorithms for compressing related data modalities [38, 43]. Compared to image and video compression, efforts to reduce the bandwidth footprint of 3D data modalities have gained less attention. Moreover, the nature of 3D data renders it a challenging problem. Typically, image or video data live on a well-defined regular grid. However, the structure, or *geometry*, of common 3D data representations such as Point Clouds (PCs) and meshes only exists on a lower-dimensional manifold embedded in the 3D world. Moreover, this is often accompanied by *attributes* that are only defined on the geometry itself.

Notably, the MPEG group has recently renewed its call for standards for 3D compression identifying point clouds as the central modality [18, 43]. To this end, geometry and attribute compression are identified as the central constituents. Geometry-based Point Cloud Compression (GPCC) and Video-based Point Cloud Compressions (VPCCs) have emerged as standards for compressing 3D PCs including attributes [43]. GPCC is based on octrees and Region-Adaptive Hierarchical Transforms (RAHT) [12]

and VPCC maps geometry and attributes onto a 2D regular grid and applies state-of-the-art video compression algorithms. Subsequently, there has been a growing effort in developing methods for compressing either the geometry, attributes or both simultaneously [6, 38].

Neural Fields (NFs) have recently been popularized for a variety of data modalities including images, videos and 3D [58]. To this end, a signal is viewed as a scalar- or vector-valued field on a coordinate space and parameterized by a neural network, typically a Multilayer Perceptron (MLP). Interestingly, there is a growing trend of applying NFs to compress various data modalities, e.g. images [13, 46], videos [8, 28, 59] or medical data [14]. Hereby, the common modus operandi is to overfit an MLP to represent a signal, e.g. image/video, and, subsequently, compress its parameters using a combination of quantization and entropy coding. Our work proposes the first NF-based 3D compression algorithm. In contrast to other geometry compression methods [38, 43], NFs have been demonstrated to represent 3D data regardless of whether it is available in form of PCs [1, 2] or meshes [10, 33]. NFs do not explicitly encode 3D data, but rather implicitly in form of Signed Distance Fields (SDFs) [33], Unsigned Distance Fields (UDFs) [10] or vector fields [39]. Therefore, one typically applies marching cubes [21, 30] on top of distances and signs/normals obtained from the NF to extract the geometry.

We show that NF-based compression using SDFs leads to state-of-the-art geometry compression. As SDFs assume watertight shapes, a general compression algorithm requires UDFs. However, vanilla UDFs lead to inferior compression performance since the non-differentiable target requires increased model capacity. To mitigate this, we apply two impactful modifications to UDFs. Specifically, we apply a suitable activation function to the output of UDFs. Further, we regularize UDFs trained on PCs. Therefore, we tune the distribution from which training points are sampled and apply an ℓ_1 -penalty on the parameters. Lastly, we demonstrate that NFs are not only a promising approach for compressing the geometry of 3D data but also its attributes by viewing attributes as a vector-valued field on the geometry.

2. Related Work

2.1. Modelling 3D Data Using Neural Fields

NFs were initially introduced to 3D shape modelling in the form of occupancy fields [9, 32] and SDFs [33]. 3D meshes are extracted from the resulting SDFs using marching cubes [30]. Further, Chibane *et al.* [10] proposed Neural Unsigned Distance fields to represent 3D shapes using UDFs and, thus, allow for modeling non-watertight shapes. They obtain shapes as PCs by projecting uniformly sampled points along the negative gradient direction of the resulting UDFs. Later, Guillard *et al.* introduced MeshUDF [21] building on Marching Cubes (MC) [30] which denotes a differentiable algorithm for converting UDFs into meshes. We instantiate our method with both SDFs and UDFs leading to a more specialized and a, respectively, more general version. More recently, Rella *et al.* proposed to parameterize the gradient field of UDFs with a neural network. Regarding the architecture of the MLP used for parameterizing NFs, Tancik *et al.* [49] solidify that positional encodings improve the ability of coordinate-based neural networks to learn high frequency content. Further, Sitzmann *et al.* [45] demonstrate that sinusoidal activation functions have a similar effect. In this work we utilize sinusoidal activation functions as well as positional encodings.

2.2. Compression Using Neural Fields

Recently, there has been an increasing interest in compressing data using NFs due to promising results and their general applicability to any coordinate-based data. Dupont *et al.* [13] were the first to propose NFs for image compression. Subsequently, there was a plethora of work extending this seminal work. Strümpler *et al.* [46] improved image compression performance and encoding runtime by combining SIREN [45] with positional encodings [49] and applying meta-learned initializations [50]. Schwarz *et al.* [42] and Dupont *et al.* [14] further expand the idea of meta-learned initializations for NF-based compression. Furthermore, various more recent works have improved upon NF-based image compression performance [11, 17, 27]. Besides images, NF-based compression has been extensively applied to videos [8, 25, 28, 31, 40, 59]. Despite the recent interest in NF-based compression, its application to compressing 3D data modalities remains scarce. Notably, there has been an increasing effort to compress 3D scenes by compressing the parameters of Neural Radiance Fields (NeRF) [5, 23, 29, 48]. However, this work directly compresses 3D data modalities (PCs/meshes) while NeRF-compression starts from 2D image observations.

2.3. 3D Data Compression

Typically, 3D compression is divided into geometry and attribute compression. We refer to Quach *et al.* [38] for a

comprehensive survey.

Geometry Compression. MPEG has identified PCs - including attributes - as a key modality for transmitting 3D information [43]. Subsequently, it introduced GPCC and VPCC for compressing the geometry and attributes captured in 3D PCs. GPCC is a 3D native algorithm which represents PCs using an efficient octree representation for geometry compression. On the other hand, VPCC maps the geometry and attributes onto a 2D grid and, then, takes advantage of video compression algorithms. Moreover, Draco [16] allows compressing PCs and meshes. For mesh compression it relies on the edge-breaker algorithm [41]. Tang *et al.* [51] take a different approach by extracting the SDF from a 3D geometry and then compressing it.

Early works on learned geometry compression use a Rate-Distortion Autoencoder (RDAE) based on 3D convolutions [19, 20, 35, 37]. Wang *et al.* [57] also apply 3D convolutions to PC compression and later introduce an improved multi-scale version based on sparse convolutions, *i.e.* Point Cloud Geometry Compression v2 (PCGCv2) [56]. PCGCv2 improves upon PC geometry compression using 3D convolutions in prior works. Thus, we use it as a learned baseline in Sec. 4.1. SparsePCGC [55] further improves upon PCGCv2¹. Tang *et al.* [52] compress watertight shapes including color attributes using Truncated Signed Distance Fields (TSDFs). Hereby, the signs of the TSDF are compressed losslessly using a learned conditional entropy model, the UDF is encoded/decoded using 3D convolutions and texture maps are compressed using a custom tracking-free UV parameterization. In contrast to all prior work on learned 3D compression, we overfit a single MLP to parameterize a single signal. While this increases the encoding time, it also drastically renders our method less vulnerable to domain shifts. Moreover, in contrast to Tang *et al.* which focuses on SDFs, we also utilize UDFs to compress non-watertight geometries. NGLOD [47] proposed to represent 3D data using feature grids with variable resolution in a parameter efficient manner. VQAD [48] further substantially improves upon NGLOD by quantizing these feature grids.

Attribute Compression. GPCC [43] compresses attributes using Region-Adaptive Hierarchical Transforms (RAHT) [12], while VPCC maps attributes onto 2D images and applies video compression algorithms. Further, Quach *et al.* [36] propose a folding-based Neural Networks (NNs) for attribute compression. Tang *et al.* [52] introduce a block-based UV parameterization and, then, applies video compression similar to VPCC. Isik *et al.* [24] demonstrate that vector-valued NFs are a promising tool for attribute compression. In contrast, this work tackles both geometry and attribute compression. Sheng *et al.* [44] and Wang *et al.* [55] compress point cloud attributes using a RDAE based on

¹Note that it is not possible to compare directly to SparsePCGC due to the absence of training code/model checkpoints.

PointNet++ [34] and, respectively, 3D convolutions.

3. Method

Generally, we fit a single NF to a 3D shape comprised of a PC/mesh and, optionally, another NF to the attributes (*e.g.* color) on the geometry. Then, we compress the parameters of the NF. Specifically, Sec. 3.1 describes how we model the geometry of 3D data - for PCs as well as meshes - using truncated Neural Distance Fields (NDFs). Further, we explain how meshes and, ultimately, PCs can be recovered from Distance Fields (DFs). Sec. 3.2 elaborates on additionally compressing attributes (*e.g.* color) of 3D data. Lastly, Sec. 3.3 describes our approach to compressing the parameters of NFs representing the underlying 3D data. Fig. 1 outlines our geometry and attribute compression pipeline.

3.1. Representing Geometries with Truncated Neural Distance Fields

We represent 3D geometries implicitly using DFs. A DF is a scalar field $DF : \mathbb{R}^3 \mapsto \mathbb{R}$ that for a given 3D geometry assigns every point $x \in \mathbb{R}^3$ the distance $d_S(x) \in \mathbb{R}_{\geq 0}$ to the closest point $x_S \in \mathbb{R}^3$ on the surface S of the geometry. We refer to such scalar fields as UDFs and omit the dependence on x , $d_S := d_S(x)$. If the underlying geometry is watertight, we can further define the signed distance $d_S \in \mathbb{R}$ which is negative inside S and positive on the outside. These instances are termed SDFs. In both cases, the surface S is implicitly defined by the level set $\{x | d_S = 0\}$ of the DF. In Sec. 4 we demonstrate that using UDFs leads to strong compression performance while being generally applicable. However, when handling watertight shapes, SDFs yield further significant improvements.

Truncated Neural Distance Fields. We parameterize d_S using NNs NF_{θ_G} with parameters θ_G - in particular MLPs mapping coordinates to the corresponding values of the scalar field similar to recent work on NFs [10, 33, 45]. Our goal is to learn compressed representations of 3D geometries in form of the parameters θ_G and, thus, it is important to limit the number of parameters. To this end, we do not train NDFs to parameterize the entire DF d_S but rather a truncated version of it. Hence, we intuitively only store the information in the DF that is necessary to recover the 3D geometry. Such a truncated DF $d_{S,T}$ is characterized by a maximal distance $d^* > 0$ and defined as

$$d_{S,T} = \begin{cases} d_S & \text{if } |d_{S,T}| \leq d^* \\ \text{sgn}(d_S)d \in \{\delta \in \mathbb{R} : |\delta| > d^*\} & \text{else.} \end{cases}$$

where $\text{sgn}(d_S)$ returns the sign of d_S . We only require $|d_{S,T}|$ to be larger than d^* but do not fix its value. Thus, the NDFs can represent the 3D geometry with fewer parameters by focusing the model’s capacity on the region closest to the surface.

Architecture. We use sinusoidal activation functions in the MLPs [45] combined with positional encodings [49]. This has been shown to improve the robustness of NFs to quantization [46]. Chibane *et al.* [10] originally proposed to parameterize UDFs using MLPs with a ReLU activation function for the output of the last layer to enforce $NF_{\theta_G} \geq 0 \forall x \in \mathbb{R}^3$. In contrast, we apply $\text{abs}(x) = |x|$ which drastically improves performance in the regime of small models (see Sec. 4.1). This originates from the fact that, unlike ReLU, $\text{abs}(x)$ allows to correctly represent a UDF using negative values prior to the last activation function. This again increases the flexibility of the model. When modeling SDFs, we apply the identity as the final activation function. More details are in the supplement.

Optimization. We train on a dataset of point-distance pairs. Following prior work [10, 45], we sample points from a mixture of three distributions - uniformly in the unit cube, uniformly from the level set and uniformly from the level set with additive Gaussian noise of standard deviation σ . This encourages learning accurate distances close to the surface. When training on PCs, we restrict ourselves to approximately uniformly distributed PCs. Non-uniform PCs can be sub/super-sampled accordingly. In contrast to prior work on compressing other data modalities using NFs [8, 13, 14, 28, 46], implicitly representing 3D geometries - in particular in the form of PCs - is susceptible to overfitting as extracting a mesh from DFs using MC requires the level set to form a 2D manifold. A NF trained on a limited number of points may collapse to a solution where the level set rather resembles a mixture of delta peaks. We counteract overfitting using two methods. We find that σ is an important parameter for the tradeoff between reconstruction quality and generalization (see Sec. 4.1). We find that for the distribution of natural shapes, the values $\sigma = 0.01$ (SDFs) and $\sigma = 0.025$ (UDFs) work well across datasets. Secondly, we penalize the ℓ_1 -norm of θ . This further has the benefit of sparsifying the parameters θ [53] and, consequently, rendering them more compressible [46]. Overall, we train NFs to predict the above truncated UDFs/SDFs using the following loss function (with $\hat{d} = NF_{\theta_G}(x)$):

$$\mathcal{L}_G(\theta_G) = \mathcal{L}_D(\theta_G) + \lambda_{\ell_1} \|\theta_G\|_1 \quad (1)$$

$$\text{where } \mathcal{L}_D(\theta_G) = \mathbb{E} \left[\left(\hat{d} - \text{sgn}(d_S) \min(|d_S|, d^*) \right)^2 \right] \text{ if}$$

$|d_S| \leq d^*$ or $|\hat{d}| \leq d^*$ and 0 otherwise.

Extracting Geometries from Distance Fields. Our compressed representation implicitly encodes the 3D surface. For comparison and visualization purposes, we need to convert it to an explicit representation, namely a PC or mesh as part of our decoding step. Obtaining a uniformly sampled PC directly from a DF is non-trivial. Hence, we initially convert the DFs into meshes in both PC compression and mesh compression scenarios. In the case of SDFs,

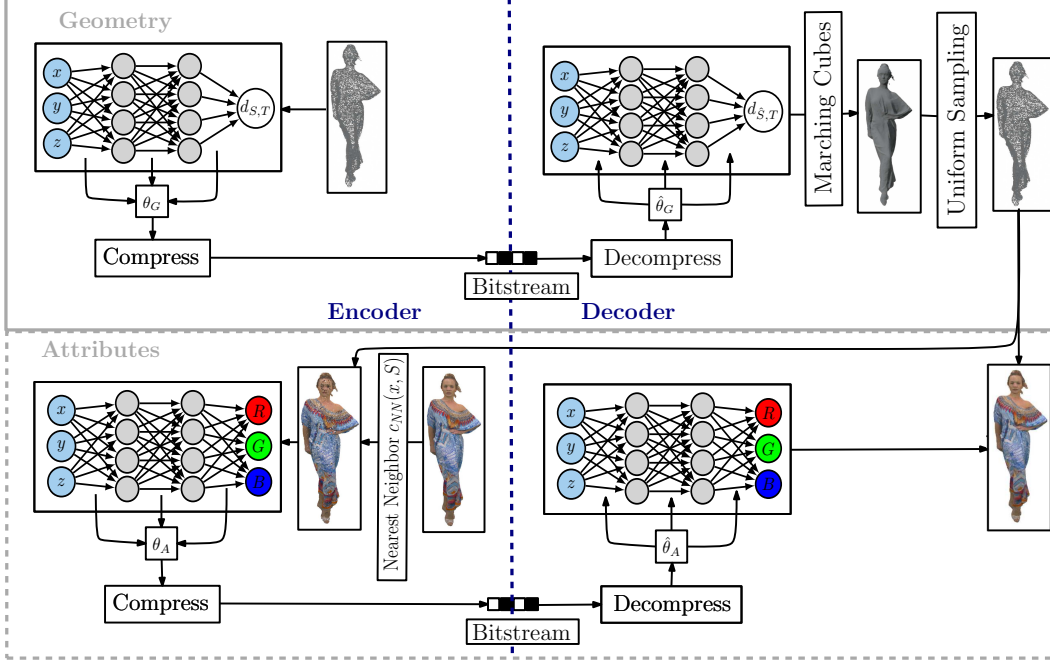


Figure 1. Overview of NF-based 3D compression. Geometry compression is in the upper part (see Sec. 3.1), while the lower part visualizes attribute compression (optional) (see Sec. 3.2). Encoding is shown on the left side. It contains two parts: a) geometry representation using NFs (see Sec. 3.1) and, resp., attribute representation (see Sec. 3.2) and b) the NF parameter compression (see Sec. 3.3).

we apply MC [30] to obtain a mesh of the 3D geometry. Further, we extract meshes from UDFs using the recently proposed differentiable MC variant MeshUDF [21]. Note that Chibane *et al.* [10] originally extracted points by projecting uniform samples along the gradient direction of UDFs. However, this leads to undesirable clustering and holes on geometries containing varying curvature. When compressing PCs, we further sample points uniformly from the extracted meshes. Notably, this is the primary reason for the inability of our compression algorithm to perform lossless compression of PCs - even in the limit of very large MLPs. However, it achieves state-of-the-art performance in the regime of strong compression ratios across various datasets on 3D compression - using PCs/meshes with/without attributes (see Sec. 4). Further, sampling PCs from the shape’s surface fundamentally limits the reconstruction quality in terms of Chamfer Distance (CD). However, unlike previous methods that approximately memorize the original PC directly, our method learns the underlying geometry.

3.2. Representing 3D Attributes with Neural Fields

Besides the geometry of 3D data, we further compress its attributes (*e.g.* color) using NFs. To this end, we follow the high level approach of other attribute compression methods and compress the attributes given the geometry [38]. Thus, after training an MLP to represent the geometry of a par-

ticular 3D shape we train a separate NF with parameters θ_A to correctly predict attributes on the approximated surface \hat{S} of the geometry $x \in \{x | NF_{\theta_G}(x) = 0\}$. Therefore, for a given point x on \hat{S} we minimize the ℓ_2 -distance to the attribute $c_{NN}(x, S)$ of the nearest neighbour on the true surface S :

$$\mathcal{L}_A(\theta_A) = \mathbb{E}_{x \in \hat{S}} \left[(NF_{\theta_A}(x) - c_{NN}(x, S))^2 \right] + \lambda_{\ell_1} \|\theta_A\|_1$$

λ_{ℓ_1} represents the strength of the regularization of θ_A and $c_{NN}(x, S) = c(\arg\min_{x' \in S} \|x - x'\|_2)$ with $c(\cdot)$ extracting the attribute at a surface point. Alternatively, one may also optimize a single NF to jointly represent a geometry and its attributes. However, then the NF has to represent attributes in regions $x \notin \hat{S}$ which wastes capacity. The supplement contains an empirical verification.

3.3. Compressing Neural Fields

In the proposed compression algorithm θ_G , and optionally θ_A , represent the 3D data. Therefore, it is important to further compress these using NN compression techniques. We achieve this by first quantizing $\theta_{G/A}$, retraining the quantized MLP to regain the lost performance and, lastly, entropy coding the resulting quantized values. Subsequently, we describe each step in detail.

Quantization. We perform scalar quantization of $\theta_{G/A}$ using a global bitwidth b which corresponds to 2^b possible

values. We use a separate uniformly-spaced quantization grid for each layer of the MLP. The layer-wise step size s_l is defined by the ℓ_∞ -norm of the parameters $\theta_{G/A}^l$ of layer l and b

$$s_l = \frac{\left\| \theta_{G/A}^l \right\|_\infty}{2^b - 1}$$

and has to be stored to recover the quantized values. Note, that the quantization grid is centered around 0 - where $\theta_{G/A}$ peaks - to improve the gain of lossless compression using entropy coding.

Quantization-Aware Retraining. We perform a few epochs of quantization-aware retraining with a much smaller learning rate. We compute gradients during quantization-aware training using the straight-through estimator [3]. We also experimented with solely training NFs using quantization-aware optimization. However, this drastically decreased convergence speed and, thus, increased the encoding time without improving performance.

Entropy Coding. Finally, we further losslessly compress the quantized parameters $\theta_{G/A}^l$ using a near optimal general purpose entropy coding algorithm².

4. Experiments

Sec. 4.1 depicts experiments on geometry compression - both for PCs and meshes. Moreover, Sec. 4.1 analyses the impact of components our compression algorithm. Sec. 4.2 investigates the performance on 3D geometry and attributes compression. We exclusively consider color attributes.

Datasets. We conduct experiments on three datasets. Firstly, we evaluate geometry compression - PC as well as mesh compression - on a set of shapes from the Stanford shape repository [54] and a subset of the MGN dataset [4] which was also used by Chibane *et al.* [10]. The former are high quality meshes consisting of both watertight and non-watertight shapes. The latter are lower quality meshes of clothing. Moreover, we conduct experiments on PCs extracted from 8i Voxelized Full Bodies (8iVFB) [15]. 8iVFB consists of four sequences of high quality colored PCs. Each PC contains between 700,000 and 1,000,000 points. We use the first frame of each sequence in our experiments. We refer to the supplement for visualizations of each dataset.

Data Preprocessing. We center each 3D shape around the origin. Then, we scale it by dividing by the magnitude of the point (PC), resp. vertex (mesh), with largest distance to the origin. For PCs, we compute the ground truth distance d_S using the nearest neighbour in the PC. For meshes, we use a CUDA implementation to convert them to SDFs [22] which we further adapt to generate UDFs. We train on points from a mixture of three distributions. 20%

are sampled uniformly $x \sim [-1, 1]^3$, 40% are sampled uniformly from the surface S and the remaining 40% are sampled uniformly from S and perturbed by additive Gaussian noise $\mathcal{N}(0; \sigma)$. For SDFs we set $\sigma = 0.01$ and for UDFs $\sigma = 0.025$ if not stated otherwise. We sample 100,000 points from S in our experiments on geometry compression on the Stanford shape repository and the MGN dataset and we use all points in the ground truth PC on 8iVFB. Color attributes are translated and scaled to the interval $[-1, 1]$.

Evaluation and Metrics. We evaluate the reconstruction quality of geometry compression using the CD. The CD is calculated between the ground truth PC and the reconstructed PC when handling PCs. For mesh compression, we report the CD between PCs uniformly sampled from the ground truth and reconstructed mesh. If not stated otherwise, we use 100,000 points on the Stanford shape repository and the MGN dataset, and all available points on 8iVFB. We evaluate the quality of reconstructed attributes using a metric based on the Peak Signal-to-Noise-Ratio (PSNR). Therefore, we compute the PSNR between the attribute of each point in the ground truth PC and its nearest neighbour in the reconstructed PC, and vice versa. The final metric is then the average between both PSNRs. Subsequently, we simply refer to this metric as PSNR. Following Strümpfer *et al.* [46], we traverse the Rate-Distortion curve by varying the width $\in \{16, 24, 32, 48, 64, 96\}$ of the MLP.

Baselines. We compare NF-based 3D compression with the non-learned baselines Draco [16], GPCC [43] and VPCC [43]. VPCC, which is based on video compression, is the non-learned state-of-the-art on compressing 3D PCs including attributes. We compare our method with the learned neural baseline PCGCv2 [56] which is the state-of-the-art RDAE based on 3D convolutions and VQAD [48] which builds quantized hierarchical feature grids. None of the baselines supports all data modalities/tasks used in our experiments. Geometry compression on meshes is only supported by Draco. On geometry compression using PCs, we compare with all baselines. Lastly, joint geometry and attribute compression is only supported by GPCC and VPCC which we evaluate on 8iVFB. Note that Draco supports normal but not color attribute compression. When sampling from meshes, we also report the theoretical minimum, *i.e.* the expected distance between independently sampled point sets.

Optimization. We train all NFs using a batch size of 10,000 for 500 epochs using a learning rate of 10^{-4} and the Adam optimizer [26]. We use $\lambda_{\ell_1} = 10^{-8}$ and $d^* = 0.1$. Each MLP contains 2 hidden layers. We follow Sitzmann *et al.* [45] and use the factor 30 as initialization scale. We use 16 fourier features as positional encodings on geometry compression and 8 on attribute compression. NFs are quantized using a bitwidth $b = 8$ and quantization-aware retraining is performed for 50 epochs using a learning rate

²<https://github.com/google/brotli>

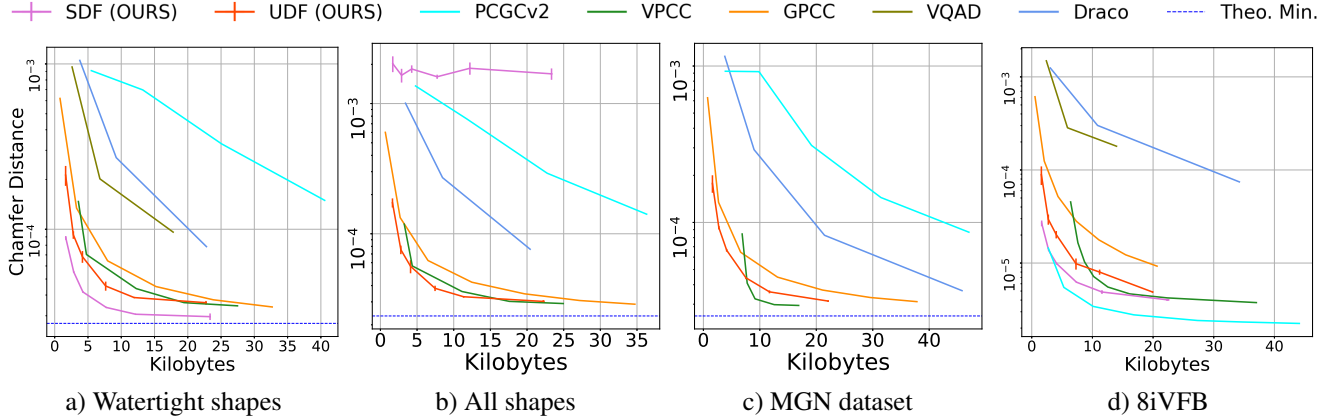


Figure 2. Rate-distortion plot for **PC compression** on the Stanford shape repository [54] (a/b), on the MGN dataset [4] (c) and 8iVFB [15] (d) depicting the average CD and number kilobytes for NFs based on UDFs/SDFs, PCGCv2, VQAD, Draco, GPCC and VPCC. PCGCv2/VQAD are learned neural baselines, and Draco, GPCC and VPCC are non-learned standards. On the Stanford shape repository we report performance on a subset only containing watertight shapes (a) and all shapes (b). We do not evaluate the performance of VQAD and NFs using SDFs on MGN dataset since it is exclusively comprised of non-watertight shapes. There is not theo. min. in (d) as we operate directly on PCs.

of 10^{-7} . Each NF is trained on a single V100 or A100.

4.1. Geometry Compression

We investigate NF-based 3D geometry compression and compare it with the baselines. We evaluate our method on PC and mesh compression and verify design choices.

Point Clouds. We evaluate PC compression on the Stanford shape repository, the MGN dataset and 8iVFB. Fig. 2 (a) & (b) depict the result on the Stanford shape repository, where we show results on the watertight subset (a) and all shapes (b), and Fig. 2 (c) & (d) contain the results on the MGN dataset and 8iVFB. Further, Fig. 3 shows qualitative results of reconstructed PCs on the Stanford shape repository. We observe that for watertight shapes on the Stanford shape repository, SDFs outperform the baselines for all levels of compression. On 8iVFB, NF-based compression is only outperformed by PCGCv2 whose performance drops steeply on other datasets. PCGCv2 was trained on ShapeNet [7] which contains artificial shapes with less details than the real scans in the Stanford shape repository and the MGN dataset. Despite its strong performance on 8iVFB, we hypothesize that PCGCv2 reacts very sensitive to the shift in the distribution of high frequency contents in the geometry. As expected the performance of SDFs deteriorates when adding non-watertight shapes since the SDF is not well defined in this case. Further, UDFs also outperform the baselines stronger compression ratios. Similarly, on the MGN dataset, where we do not evaluate SDFs as all shapes are non-watertight, and on 8iVFB UDFs perform well for strong compression ratios and are only outperformed by VPCC on weaker compression ratios and by PCGCv2 on 8iVFB.

Table 1. We report the average encoding (top) and decoding (bottom) runtime in [s] on the Stanford shape repository of Draco, PCGCv2, GPCC, VPCC, VQAD and our approach based on UDFs. Draco, GPCC and VPCC are evaluated on a CPU, while NF-based compression, VQAD and PCGCv2 are evaluated on a single V100.

Draco	PCGCv2	GPCC	VPCC	VQAD	OURS
0.06	0.50	0.26	46.1	172	500
0.04	0.96	0.04	2.3	3.3	1.6

Meshes. Fig. 4 (a) & (b) contains quantitative mesh compression results on the Stanford shape repository and the MGN dataset. Moreover, we refer to the supplement for qualitative results of reconstructed meshes. We only evaluate UDFs since both datasets contain non-watertight shapes. We find that NF-based compression outperforms Draco on more complex meshes (Stanford shape repository), while Draco can outperform UDFs on simpler meshes (MGN dataset). This is reasonable since the meshes in the MGN dataset contain large planar regions which benefits the edge-breaker algorithm [41] used by Draco as it is easier to represent such regions with only a few triangles.

Architecture Choices. We investigate the impact of using truncated DFs and applying the abs activation function to the output of UDFs. Fig. 5 (a) depicts the result. We observe that both, truncation and abs activation function, are essential for UDFs with strong compression performance. Note that Chibane *et al.* [10] used ReLU as the final activation function. We refer to the supplement for a demonstration that ReLU performs similar to a linear activation

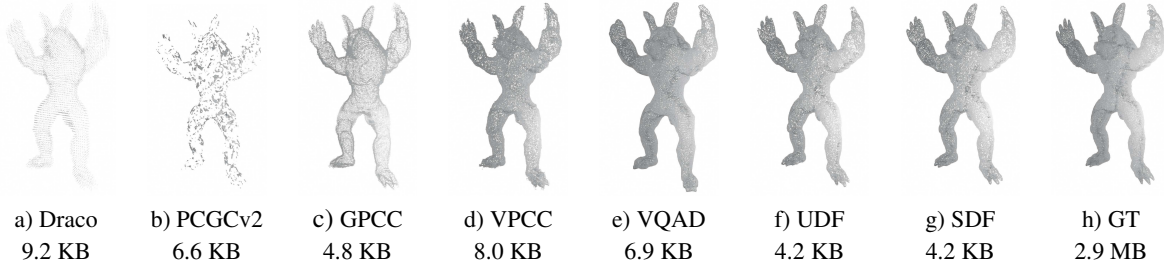


Figure 3. We depict qualitative results on "Armadillo" of the Stanford shape repository for Draco (a), PCGCv2 (b), GPCC (c), VPCC (d), Vector Quantized Autodecoder (e), UDFs/SDFs (f/g) and the ground truth (h).

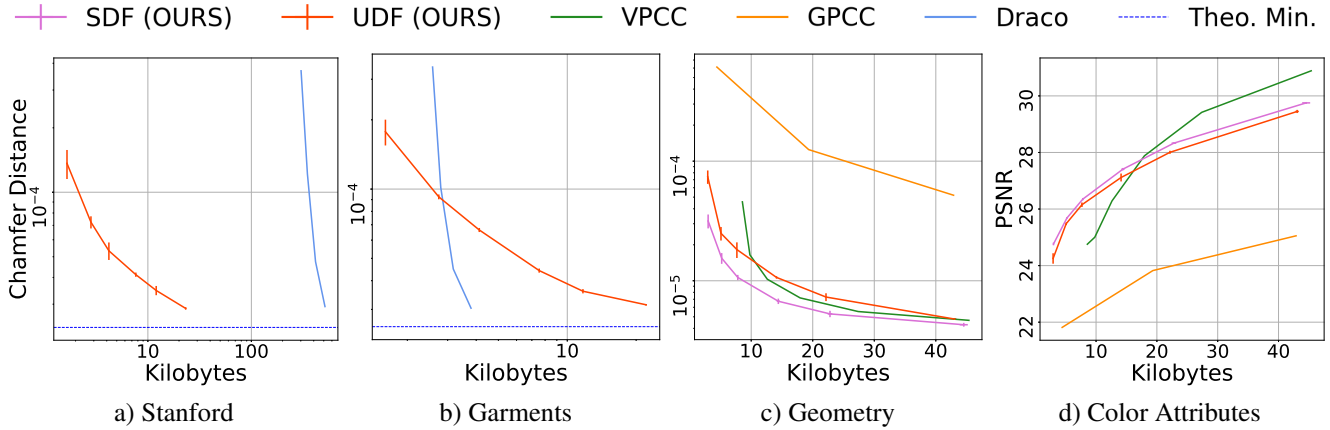


Figure 4. Rate-distortion plot for **mesh compression** on the Stanford shape repository [54] (a) and the MGN dataset [4] (b), and for **geometry and attribute compression** (c/d) on 8iVFB [15]. On mesh compression, we report the average CD and kilobytes for NFs based on UDFs/SDFs and Draco. We do not evaluate the performance of NFs using SDFs due to non-watertight shapes. In (c)/(d), we report the average CD/PSNR and kilobytes for NFs-based on UDFs/SDFs, GPCC and VPCC. There is no theo. min. in (c) as we use the PCs.

function.

Regularization. We demonstrate the impact of regularization in Fig. 5 (b) & (c). Adding Gaussian noise $\sigma \sim \mathcal{N}(0; 0.025)$ and applying an ℓ_1 -penalty to the parameters θ_G increasingly improves performance for larger NFs. This is expected as larger NNs require more regularization to prevent overfitting which is a problem for NF-based compression of 3D geometries - in contrast to other data modalities.

UDF Parameter Initialization. Interestingly, we observe that the CD of NF-based compression using UDFs has a large variance. In fact, the primary source of this randomness is the parameter initialization which we find by optionally fixing the random seed of the dataset and parameter initialization. For this result we refer the reader to the supplement. Moreover, qualitatively we find in Fig. 5 (d) that UDFs which converge to a SDFs prior to the abs activation function yield lower CD.

Runtime. We compare the encoding and decoding runtime of NF-based compression with the baselines (see Tab. 1). The encoding runtime of our approach is slower compared to the baselines since it needs to fit a NN to each

instance. Notably, this can be improved using meta-learned initializations [46] Interestingly, compared to VPCC, which is the only baseline that is competitive in terms of compression performance on weaker compression ratios, NF-based compression is competitive if decoding is performed on a GPU. This renders NF-based compression practical when a 3D shape needs to be decoded many more times than encoded.

4.2. Attribute Compression

Furthermore, we evaluate NF-based compression on PCs containing color attributes on 8iVFB and compare it with GPCC and VPCC. Fig. 4 (c) & (d) show quantitative and Fig. 6 qualitative results. NF-based compression using SDF outperforms both baselines on geometry compression. UDFs outperform VPCC for strong compression ratios. On attribute compression SDFs and UDFs outperform GPCC by a large margin, but VPCC only for stronger compression ratios. We show in the supplement that jointly compressing geometry and attributes leads to worse performance.

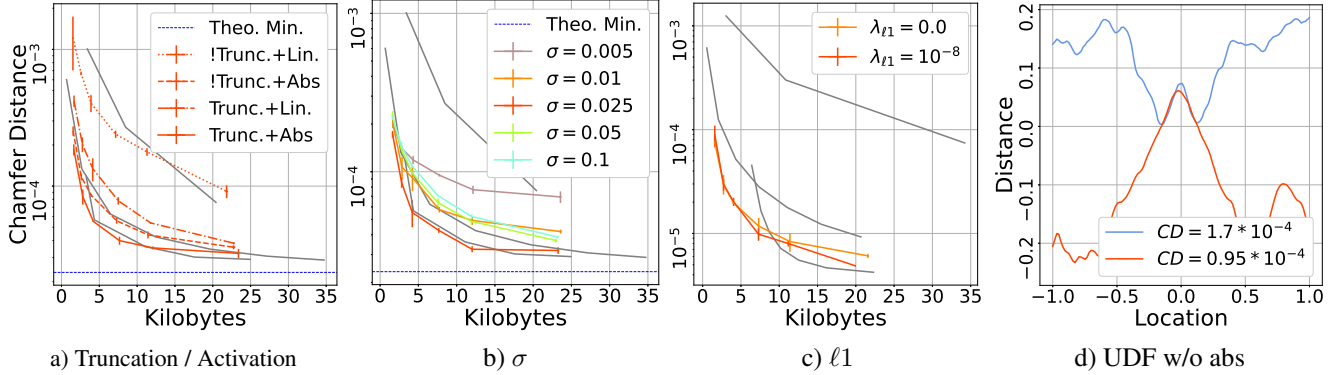


Figure 5. Impact of using truncated (Trunc.) DFs and the abs activation function (a), regularization effect of the standard deviation σ added to points during training (b) on the Stanford shape repository [54]. (c) depicts the impact of the ℓ_1 penalty on 8iVFB. We plot Draco, VPCC and GPCC in the background for reference (grey). We observe that UDFs demonstrate the strongest performance when combining truncated unsigned distance fields with the abs activation function (a), when adding noise of standard deviation $\sigma = 0.025$ to the raw PC (b) and when applying an ℓ_1 -penalty to its parameters. We further visualize a 1D-cut through the center of the shape *Armadillo* of the dataset Stanford shape repository for two independently trained UDFs with a hidden dimension of 16 (d). We observe that the UDF which converges to a SDF (red) prior to the abs activation function yields lower CD.

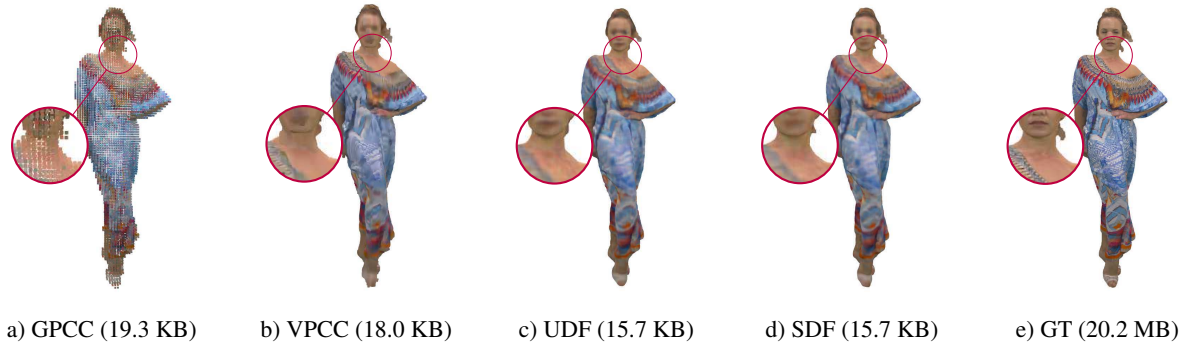


Figure 6. "Longdress" of 8iVFB for GPCC (a), VPCC (b), UDFs/SDFs (c/d) and the target (e).

5. Discussion

We proposed an algorithm for compressing the geometry as well as attributes of 3D data using NFs. We introduced two variants - one specialized to watertight shapes based on SDFs and another more general approach based on UDFs (see Sec. 3). For watertight shapes SDFs demonstrate strong geometry compression performance across all compression ratios (see Sec. 4.1). UDFs perform well on geometry compression - in particular for stronger compression ratios. However, VPCC can outperform UDFs on weaker compression ratios. Notably, the learned neural baseline PCGCv2s shows strong performance on 8iVFB, but suffers from large performance drops on Stanford shape repository and MGN dataset. This highlights another strength of NF-based neural compression - it does not exhibit the sensitivity to domain shifts of other neural compression algorithms. On attribute compression (see Sec. 4.2) SDFs as well as UDFs outperform both baselines for stronger compression

ratios, while VPCC performs better when less compression is required.

Interestingly, we observed in Sec. 4.1 that the decoding runtime of NF-based compression is competitive on a GPU. This is in line with recent findings on NF-based video compression [28]. However, the encoding runtime remains one order of magnitude larger than the next slowest method (VPCC). This gap can potentially be closed when using meta-learned initializations which have been found to improve NF-based image compression [14, 46] and speed up convergence by a factor of 10 [46].

Furthermore, we found that the performance of UDFs strongly depends on the parameter initialization (see Sec. 4.1). When using the abs activation function, UDFs are flexible regarding the values they predict prior to it. On watertight shapes, UDFs can converge to a function predicting the same sign inside and outside or one that predicts different signs. In presence of a sign flip, UDFs perform

better. Thus, a promising direction for improving the more general compression method based on UDFs are novel initialization methods beyond the one provided in Sitzmann *et al.* [45]. Notably, one line of work aims at learning SDFs from raw point clouds by initializing NFs such that they approximately resemble an SDF of an r-ball after initialization [1, 2]. However, none of these methods work when using positional encodings which are necessary for strong performance.

References

- [1] Matan Atzmon and Yaron Lipman. Sal: Sign agnostic learning of shapes from raw data. In *Proceedings of the IEEE/CVF Conference on Computer Vision and Pattern Recognition*, pages 2565–2574, 2020.
- [2] Matan Atzmon and Yaron Lipman. Sald: Sign agnostic learning with derivatives. *9th International Conference on Learning Representations*, 2021.
- [3] Yoshua Bengio, Nicholas Léonard, and Aaron Courville. Estimating or propagating gradients through stochastic neurons for conditional computation. *arXiv preprint arXiv:1308.3432*, 2013.
- [4] Bharat Lal Bhatnagar, Garvita Tiwari, Christian Theobalt, and Gerard Pons-Moll. Multi-garment net: Learning to dress 3d people from images. In *IEEE International Conference on Computer Vision (ICCV)*. IEEE, 2019.
- [5] Thomas Bird, Johannes Ballé, Saurabh Singh, and Philip A Chou. 3d scene compression through entropy penalized neural representation functions. In *2021 Picture Coding Symposium (PCS)*, pages 1–5. IEEE, 2021.
- [6] Chao Cao, Marius Preda, and Titus Zaharia. 3d point cloud compression: A survey. In *The 24th International Conference on 3D Web Technology*, pages 1–9, 2019.
- [7] Angel X. Chang, Thomas Funkhouser, Leonidas Guibas, Pat Hanrahan, Qixing Huang, Zimo Li, Silvio Savarese, Manolis Savva, Shuran Song, Hao Su, Jianxiong Xiao, Li Yi, and Fisher Yu. ShapeNet: An Information-Rich 3D Model Repository. Technical Report arXiv:1512.03012 [cs.GR], Stanford University — Princeton University — Toyota Technological Institute at Chicago, 2015.
- [8] Hao Chen, Bo He, Hanyu Wang, Yixuan Ren, Ser Nam Lim, and Abhinav Shrivastava. Nerv: Neural representations for videos. *Advances in Neural Information Processing Systems*, 34:21557–21568, 2021.
- [9] Zhiqin Chen and Hao Zhang. Learning implicit fields for generative shape modeling. In *Proceedings of the IEEE/CVF Conference on Computer Vision and Pattern Recognition*, pages 5939–5948, 2019.
- [10] Julian Chibane, Gerard Pons-Moll, et al. Neural unsigned distance fields for implicit function learning. *Advances in Neural Information Processing Systems*, 33:21638–21652, 2020.
- [11] Bharath Bhushan Damodaran, Muhammet Balcilar, Franck Galpin, and Pierre Hellier. Rqat-inr: Improved implicit neural image compression. *arXiv preprint arXiv:2303.03028*, 2023.
- [12] Ricardo L De Queiroz and Philip A Chou. Compression of 3d point clouds using a region-adaptive hierarchical transform. *IEEE Transactions on Image Processing*, 25(8):3947–3956, 2016.
- [13] Emilien Dupont, Adam Golinski, Milad Alizadeh, Yee Whye Teh, and Arnaud Doucet. Coin: Compression with implicit neural representations. *arXiv preprint arXiv:2103.03123*, 2021.
- [14] Emilien Dupont, Hrushikesh Loya, Milad Alizadeh, Adam Golinski, Y Whye Teh, and Arnaud Doucet. Coin++: Neural compression across modalities. *Transactions on Machine Learning Research*, 2022(11), 2022.
- [15] Eugene d’Eon, Bob Harrison, Taos Myers, and Philip A Chou. 8i voxelized full bodies-a voxelized point cloud dataset. *ISO/IEC JTC1/SC29 Joint WG11/WG1 (MPEG/JPEG) input document WG11M40059/WG1M74006*, 7(8):11, 2017.
- [16] Frank Galligan, Michael Hemmer, Ondrej Stava, Fan Zhang, and Jamieson Brett. Google/draco: a library for compressing and decompressing 3d geometric meshes and point clouds, 2018.
- [17] Harry Gao, Weijie Gan, Zhixin Sun, and Ulugbek S Kamilov. Sinco: A novel structural regularizer for image compression using implicit neural representations. *arXiv preprint arXiv:2210.14974*, 2022.
- [18] 3D Graphics. Call for proposals for point cloud compression v2. *ISO/IEC JTC1/SC29/WG11 MPEG, N 1676*, 2017.
- [19] André FR Guarda, Nuno MM Rodrigues, and Fernando Pereira. Deep learning-based point cloud coding: A behavior and performance study. In *2019 8th European Workshop on Visual Information Processing (EUVIP)*, pages 34–39. IEEE, 2019.
- [20] André FR Guarda, Nuno MM Rodrigues, and Fernando Pereira. Deep learning-based point cloud geometry coding: Rd control through implicit and explicit quantization. In *2020 IEEE International Conference on Multimedia & Expo Workshops (ICMEW)*, pages 1–6. IEEE, 2020.
- [21] Benoit Guillard, Federico Stella, and Pascal Fua. Meshudf: Fast and differentiable meshing of unsigned distance field networks. In *Computer Vision—ECCV 2022: 17th European Conference, Tel Aviv, Israel, October 23–27, 2022, Proceedings, Part III*, pages 576–592. Springer, 2022.
- [22] Zekun Hao, Hadar Averbuch-Elor, Noah Snavely, and Serge Belongie. Dualsdf: Semantic shape manipulation using a two-level representation. In *Proceedings of the IEEE/CVF Conference on Computer Vision and Pattern Recognition*, 2020.
- [23] Berivan Isik. Neural 3d scene compression via model compression. *arXiv preprint arXiv:2105.03120*, 2021.
- [24] Berivan Isik, Philip Chou, Sung Jin Hwang, Nicholas Johnston, and George Toderici. Lvac: Learned volumetric attribute compression for point clouds using coordinate based networks. *Frontiers in Signal Processing*, page 65, 2021.
- [25] Subin Kim, Sihyun Yu, Jaeho Lee, and Jinwoo Shin. Scalable neural video representations with learnable positional features. In *Advances in Neural Information Processing Systems*.

- [26] Diederik P Kingma and Jimmy Ba. Adam: A method for stochastic optimization. *arXiv preprint arXiv:1412.6980*, 2014.
- [27] Théo Ladune, Pierrick Philippe, Félix Henry, and Gordon Clare. Cool-chic: Coordinate-based low complexity hierarchical image codec. *arXiv preprint arXiv:2212.05458*, 2022.
- [28] Joo Chan Lee, Daniel Rho, Jong Hwan Ko, and Eunbyung Park. Ffnerv: Flow-guided frame-wise neural representations for videos. *arXiv preprint arXiv:*, 2022.
- [29] Lingzhi Li, Zhen Shen, Zhongshu Wang, Li Shen, and Liefeng Bo. Compressing volumetric radiance fields to 1 mb. In *Proceedings of the IEEE/CVF conference on computer vision and pattern recognition*, 2023.
- [30] William E Lorensen and Harvey E Cline. Marching cubes: A high resolution 3d surface construction algorithm. *ACM siggraph computer graphics*, 21(4):163–169, 1987.
- [31] Shishira R Maiya, Sharath Girish, Max Ehrlich, Hanyu Wang, Kwot Sin Lee, Patrick Poirson, Pengxiang Wu, Chen Wang, and Abhinav Shrivastava. Nirvana: Neural implicit representations of videos with adaptive networks and autoregressive patch-wise modeling. *arXiv preprint arXiv:2212.14593*, 2022.
- [32] Lars Mescheder, Michael Oechsle, Michael Niemeyer, Sebastian Nowozin, and Andreas Geiger. Occupancy networks: Learning 3d reconstruction in function space. In *Proceedings of the IEEE/CVF conference on computer vision and pattern recognition*, pages 4460–4470, 2019.
- [33] Jeong Joon Park, Peter Florence, Julian Straub, Richard Newcombe, and Steven Lovegrove. DeepSDF: Learning continuous signed distance functions for shape representation. In *Proceedings of the IEEE/CVF conference on computer vision and pattern recognition*, pages 165–174, 2019.
- [34] Charles Ruizhongtai Qi, Li Yi, Hao Su, and Leonidas J Guibas. Pointnet++: Deep hierarchical feature learning on point sets in a metric space. *Advances in neural information processing systems*, 30, 2017.
- [35] Maurice Quach, Giuseppe Valenzise, and Frederic Dufaux. Learning convolutional transforms for lossy point cloud geometry compression. In *2019 IEEE international conference on image processing (ICIP)*, pages 4320–4324. IEEE, 2019.
- [36] Maurice Quach, Giuseppe Valenzise, and Frederic Dufaux. Folding-based compression of point cloud attributes. In *2020 IEEE International Conference on Image Processing (ICIP)*, pages 3309–3313. IEEE, 2020.
- [37] Maurice Quach, Giuseppe Valenzise, and Frederic Dufaux. Improved deep point cloud geometry compression. In *2020 IEEE 22nd International Workshop on Multimedia Signal Processing (MMSP)*, pages 1–6. IEEE, 2020.
- [38] Maurice Quach, Jiahao Pang, Dong Tian, Giuseppe Valenzise, and Frédéric Dufaux. Survey on deep learning-based point cloud compression. *Frontiers in Signal Processing*, 2022.
- [39] Edoardo Mello Rella, Ajad Chhatkuli, Ender Konukoglu, and Luc Van Gool. Neural vector fields for surface representation and inference. *arXiv preprint arXiv:2204.06552*, 2022.
- [40] Daniel Rho, Junwoo Cho, Jong Hwan Ko, and Eunbyung Park. Neural residual flow fields for efficient video representations. In *Proceedings of the Asian Conference on Computer Vision*, pages 3447–3463, 2022.
- [41] Jarek Rossignac. Edgebreaker: Connectivity compression for triangle meshes. *IEEE transactions on visualization and computer graphics*, 5(1):47–61, 1999.
- [42] Jonathan Schwarz and Yee Whye Teh. Meta-learning sparse compression networks. *Transactions of Machine Learning Research*, 2022.
- [43] Sebastian Schwarz, Marius Preda, Vittorio Baroncini, Madhukar Budagavi, Pablo Cesar, Philip A Chou, Robert A Cohen, Maja Krivokuća, Sébastien Lasserre, Zhu Li, et al. Emerging mpeg standards for point cloud compression. *IEEE Journal on Emerging and Selected Topics in Circuits and Systems*, 9(1):133–148, 2018.
- [44] Xihua Sheng, Li Li, Dong Liu, Zhiwei Xiong, Zhu Li, and Feng Wu. Deep-pcac: An end-to-end deep lossy compression framework for point cloud attributes. *IEEE Transactions on Multimedia*, 24:2617–2632, 2021.
- [45] Vincent Sitzmann, Julien Martel, Alexander Bergman, David Lindell, and Gordon Wetzstein. Implicit neural representations with periodic activation functions. *Advances in Neural Information Processing Systems*, 33:7462–7473, 2020.
- [46] Yannick Strümpfer, Janis Postels, Ren Yang, Luc Van Gool, and Federico Tombari. Implicit neural representations for image compression. In *Computer Vision–ECCV 2022: 17th European Conference, Tel Aviv, Israel, October 23–27, 2022, Proceedings, Part XXVI*, pages 74–91. Springer, 2022.
- [47] Towaki Takikawa, Joey Litalien, Kangxue Yin, Karsten Kreis, Charles Loop, Derek Nowrouzezahrai, Alec Jacobson, Morgan McGuire, and Sanja Fidler. Neural geometric level of detail: Real-time rendering with implicit 3d shapes. In *Proceedings of the IEEE/CVF Conference on Computer Vision and Pattern Recognition*, pages 11358–11367, 2021.
- [48] Towaki Takikawa, Alex Evans, Jonathan Tremblay, Thomas Müller, Morgan McGuire, Alec Jacobson, and Sanja Fidler. Variable bitrate neural fields. In *ACM SIGGRAPH 2022 Conference Proceedings*, pages 1–9, 2022.
- [49] Matthew Tancik, Pratul Srinivasan, Ben Mildenhall, Sara Fridovich-Keil, Nithin Raghavan, Utkarsh Singhal, Ravi Ramamoorthi, Jonathan Barron, and Ren Ng. Fourier features let networks learn high frequency functions in low dimensional domains. *Advances in Neural Information Processing Systems*, 33:7537–7547, 2020.
- [50] Matthew Tancik, Ben Mildenhall, Terrance Wang, Divi Schmidt, Pratul P Srinivasan, Jonathan T Barron, and Ren Ng. Learned initializations for optimizing coordinate-based neural representations. In *Proceedings of the IEEE/CVF Conference on Computer Vision and Pattern Recognition*, pages 2846–2855, 2021.
- [51] Danhang Tang, Mingsong Dou, Peter Lincoln, Philip Davidson, Kaiwen Guo, Jonathan Taylor, Sean Fanello, Cem Keskin, Adarsh Kowdle, Sofien Bouaziz, et al. Real-time compression and streaming of 4d performances. *ACM Transactions on Graphics (TOG)*, 37(6):1–11, 2018.
- [52] Danhang Tang, Saurabh Singh, Philip A Chou, Christian Hane, Mingsong Dou, Sean Fanello, Jonathan Taylor, Philip

- Davidson, Onur G Guleryuz, Yinda Zhang, et al. Deep implicit volume compression. In *Proceedings of the IEEE/CVF conference on computer vision and pattern recognition*, pages 1293–1303, 2020.
- [53] Robert Tibshirani. Regression shrinkage and selection via the lasso. *Journal of the Royal Statistical Society: Series B (Methodological)*, 58(1):267–288, 1996.
- [54] Greg Turk and Marc Levoy. Zippered polygon meshes from range images. In *Proceedings of the 21st annual conference on Computer graphics and interactive techniques*, pages 311–318, 1994.
- [55] Jianqiang Wang and Zhan Ma. Sparse tensor-based point cloud attribute compression. In *2022 IEEE 5th International Conference on Multimedia Information Processing and Retrieval (MIPR)*, pages 59–64. IEEE, 2022.
- [56] Jianqiang Wang, Dandan Ding, Zhu Li, and Zhan Ma. Multi-scale point cloud geometry compression. In *2021 Data Compression Conference (DCC)*, pages 73–82. IEEE, 2021.
- [57] Jianqiang Wang, Hao Zhu, Haojie Liu, and Zhan Ma. Lossy point cloud geometry compression via end-to-end learning. *IEEE Transactions on Circuits and Systems for Video Technology*, 31(12):4909–4923, 2021.
- [58] Yiheng Xie, Towaki Takikawa, Shunsuke Saito, Or Litany, Shiqin Yan, Numair Khan, Federico Tombari, James Tompkin, Vincent Sitzmann, and Srinath Sridhar. Neural fields in visual computing and beyond. *Computer Graphics Forum*, 2022.
- [59] Yunfan Zhang, Ties van Rozendaal, Johann Brehmer, Markus Nagel, and Taco Cohen. Implicit neural video compression. In *ICLR Workshop on Deep Generative Models for Highly Structured Data*, 2021.